Polarization-sensitive optoacoustic tomography of optically diffuse tissues

Daniel Razansky,[1,2,3,*] Claudio Vinegoni,[3,4] and Vasilis Ntziachristos[1,2,3]

[1]*Institute for Biological and Medical Imaging, Helmholtz Zentrum München, Ingolstädter Landstraße 1, D-85764 Neuherberg, Germany*

[2]*School of Medicine and School of Electrical Engineering, Technische Universität München, Troger Strasse 32, D-81675 München, Germany*

[3]*Laboratory for Bio-optics and Molecular Imaging, Center for Molecular Imaging Research, Massachusetts General Hospital and Harvard Medical School, 149 13th Street, Charlestown, Massachusetts 02129, USA*

[4]*Now with the Center for Systems Biology, Massachusetts General Hospital and Harvard Medical School, Richard B. Simches Research Center, 185 Cambridge Street, Boston, Massachusetts 02114, USA*

**Corresponding author: daniel.razansky@helmholtz-muenchen.de*

Received June 10, 2008; revised August 12, 2008; accepted August 25, 2008; posted September 10, 2008 (Doc. ID 97265); published October 9, 2008

Polarization is indicative of material anisotropy, a property that reveals structural orientation information of molecules inside the material. Herein we investigate whether polarization can be detected optoacoustically in scattering and absorbing tissues. Using a laboratory prototype of polarization-sensitive optoacoustic tomography, we demonstrate high-resolution reconstructions of dichroism contrast deep in optically diffusive tissue-mimicking phantoms. The technique is expected to enable highly accurate imaging of polarization contrast in tissues, far beyond the current capabilities of pure optical polarization-imaging approaches.

OCIS codes: 170.3880, 170.5120, 170.7050, 290.5855.

Optoacoustic (or photoacoustic) biological imaging and tomography are based on exploiting the thermoacoustic phenomenon generated by fast local temperature changes inside tissues owing to light absorption by tissue chromophores or exogeneous agents [1–6]. Typically, nanosecond-duration intense laser pulses are used that are locally absorbed within the sample under investigation and converted into heat, leading to transient thermoelastic expansion, giving rise to acoustic waves. The amplitude of the ultrasound wave is proportional to the product between local fluence and the optical absorption coefficient at the imaging wavelength, whereas a wideband ultrasound wave is generated with spectral content that relates to the spatial extend of the local light-pulse absorption. Optoacoustic imaging therefore combines diffusion-free ultrasonic imaging resolution with optical contrast. As a consequence, optoacoustics has been used to image hemoglobin-based contrast in functional brain imaging [2], for vasculature mapping in angiogenesis studies [3], resolving fluorescent markers in tissue [4], or imaging of molecularly targeted plasmonic gold nanoparticles [5], all those attaining high potential for molecular imaging applications.

In this Letter we hypothesize that polarization contrast could be similarly detected based on the preferential absorption of polarized light in tissues. Polarization contrast is characterized by anisotropic tissue properties relating to structural elements associated with development and function, e.g., muscle-cell orientation [7], birefringence of cytoskeletal filaments [8], linear dichroism of the cornea [9] or disease, e.g., in Alzheimer-associated amyloid-β plaque deposits [10]. However, during propagation in a diffusive medium, polarized light is found to lose its propagation direction and polarization properties [11]. This is because scattering events that arise on a length scale equal to the transport mean-free path tend to create an isotropization of both the direction and the polarization, with an isotropization length that is much larger than the transport mean-free path. This quantity is a function of the diffusive medium properties, i.e., refractive index and scatterers' size. Regardless, optical imaging of polarized structures have been proven feasible for many mean-free paths in diffuse tissue, albeit with low diffusion-limited resolution [12].

Optoacoustic imaging of polarized structures leads to important advantages, since signals created by light absorption are detected ultrasonically, thus depolarization due to optical path from target back to detector is eliminated. In this way the possible propagation distance for which polarization can be detected virtually doubles. Moreover, since image formation is not directly related to the diffusion path length as in pure diffusive optics, superior spatial resolution can be achieved. To investigate whether we could detect polarization contrast using optoacoustics, a tunable optical parametric oscillator laser (Vibrant-532-I, Opotek Inc., Carlsbad, California, USA) with a pulse duration below 10 ns and a repetition frequency of 20 Hz was employed. For the ultrasonic detection we used a broadband transducer with a central frequency of 3.7 MHz and 75% bandwidth (Model V382, Panametrics-NDT, Waltham, Massachusetts, USA) cylindrically focused in the image plane. The recorded signals were amplified, digitized, and averaged by an acquisition card with 100 mega samples per second (NI PCI-5122, National Instruments Corp., Austin, Texas, USA) and 14-bit digital resolution.

In the first set of experiments [Fig. 1(a)], a 0.5-mm-thick polarized film F was incorporated at a depth d

within a turbid medium consisting of 3% (by volume) of Lyposin-II-10% (Hospira Inc., Lake Forest, Illinois, USA), which provided reduced scattering coefficient of $\mu_s' = 2.5\ \text{cm}^{-1}$. The input laser beam was first vertically polarized by way of a polarizer P1, and its polarization direction was then rotated using a half-wave plate HP aligned parallel to it ($\alpha = 0°$). The polarized film F in the medium was oriented such that its polarization axis was parallel to the polarizer P1. The optoacoustic signals at various polarization angles and film depths were subsequently recorded. The results for the relative peak-to-peak magnitude of the optoacoustic signals versus polarization angle and target depth are depicted in Fig. 1(b). The polarized film F acts as an analyzer for the incoming laser beam with the optoacoustic signal following the Malus' law with a $\sin^2$ dependence on twice the half-wave-plate angle α. For $\alpha = 45°$, i.e., with the half-wave plate making an angle of 45° with respect to the polarizer P1, the input light polarization is horizontally aligned, corresponding to a minimum in transmission (maximum optoacoustic signal) through the polarized film F. Owing to light scattering, as the film depth increases, the light undergoes depolarization, and therefore the relative changes in the optoacoustic signal due to polarization rotation are decreasing. For comparison, we used a CCD camera [Fig. 2(a)] in order to measure depolarization of light as it passes through a turbid slab of varying thickness d having scattering properties equal to the ones of the previous experiment, with the polarizer P1 and P2 aligned parallelly. The results are presented in Fig. 2(b) and are in good agreement with the optoacoustic measurements from Fig. 1(b), with here the signal intensity presenting the similar $\sin^2$ dependence on the angle α. Note that in both experiments the extinction ratio at depth zero is not equal to 100%, because the wave plate was a half-wave plate at a wavelength different by 50 nm from the one used in the experiment.

In the second set of experiments we investigated whether we could form polarization-sensitive images using optoacoustic tomography. For this purpose we

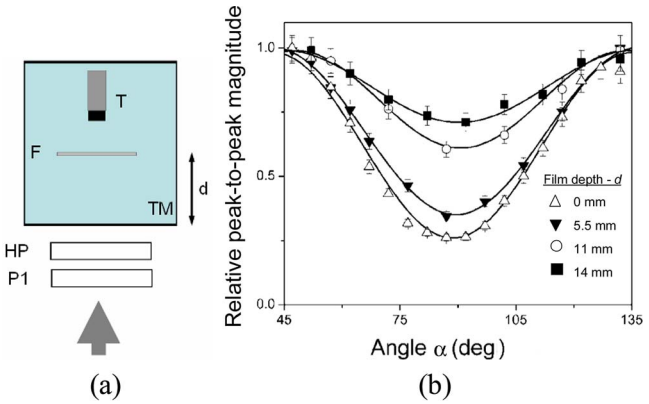

Fig. 1. (Color online) Optoacoustic polarization measurements. (a) Diagram of the experimental setup: P1, linear polarizer; HP, half-wave plate; F, polarized film; TM, turbid medium; T, transducer. (b) Relative peak-to-peak magnitude of the recorded optoacoustic response versus the angle α of the half-wave plate with respect to the polarizer P1 for different depths of the film F.

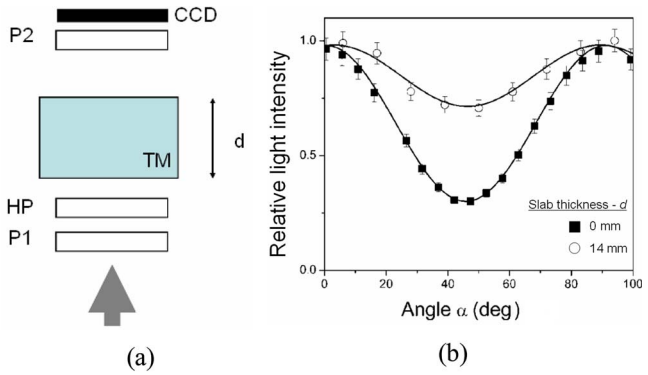

Fig. 2. (Color online) Optical polarization measurements. (a) Diagram of the experimental setup; (b) relative peak intensity recorded by the CCD camera versus the angle α of the half-wave plate with respect to the linear polarizer P1, for two different thicknesses of turbid slab.

utilized a multispectral optoacoustic tomography setup, previously developed in [4], fitted with a polarizer and a half-wave plate as in Fig 1(a), in order to reconstruct images from a tissue-mimicking phantom having polarization contrast. The phantom was created by molding 0.006% (by volume) of India ink (Higgins, Sanford Bellwood, Illinois, USA) and 24% of Lyposin-II-10% in agar, assuming a 10-mm-diameter cylindrical shape (3 cm long), attaining background optical absorption of $\mu_a = 0.3\ \text{cm}^{-1}$ and reduced scattering coefficient of $\mu_s' = 20\ \text{cm}^{-1}$. To create polarization contrast, a 3-mm-wide strip of polarized film was introduced in the middle of the phantom. In addition, a cylindrical insertion having 0.8 mm diameter and higher optical absorption coefficient of $\mu_a = 1\ \text{cm}^{-1}$ was introduced as control. The phantom was fixed on the rotation stage (Newport Corp., Irvine, California, USA) and rotated 360° with 3° steps to allow for two-dimensional image reconstruction using filtered back-projection. Details of the inversion algorithm can be found in [6]. The phantom was illuminated from the side to resemble whole-body small-animal imaging scenario, as shown in Fig. 3(a). In this way the polarization angle of the beam with respect to polarized film remained constant throughout 360° rotation. Optoacoustic images for the two polarization states are presented in Figs. 3(b) and 3(c) and apparently attain similar appearance, providing no useful information on the actual polarization contrast of the internal structures. In contrast, the difference image [Fig. 3(d)] clearly suppresses other structures and emphasizes the polarized strip with both high contrast and high spatial resolution on the order of 150 μm, corresponding to the useful bandwidth of the ultrasonic transducer (5 Mhz).

It should be noted that the method is expected to be mostly sensitive to anisotropic effects arising from dichroism (or what is sometimes called biattenuance) rather than birefringence. Dichroism relates to materials (or tissue) that present light absorption dependent on the state of polarization of the light. It was already mentioned, however, that the detected optoacoustic response is proportional to a product between local fluence and optical absorption coefficient. The assumption was therefore that in most real bio-

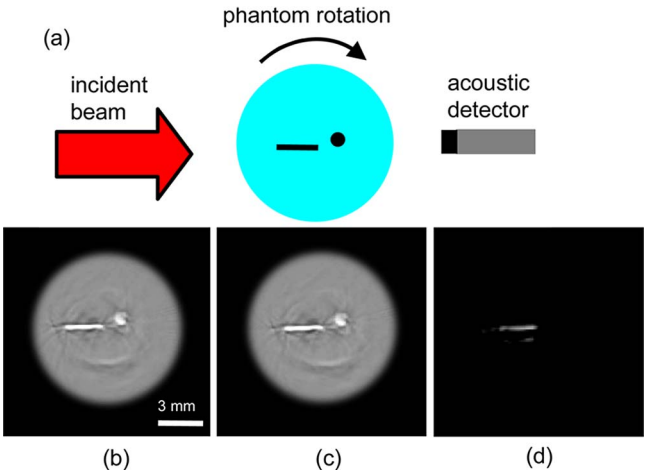

Fig. 3. (Color online) Polarization-sensitive optoacoustic tomography (PSOT) images of a thin polarized film incorporated into heterogeneous tissue-mimicking phantom. (a) Diagram of the measurement configuration; (b) and (c) are the regular optoacoustic images for polarization angles providing maximal and minimal optoacoustic response from the film, respectively. (d) Difference image between (b) and (c).

logical tissues the anisotropic effects are generally relatively weak and localized, in which case image artifacts due to dependence of local fluence distribution on polarization will be minimal. On the other hand, in cases of significant scattering anisotropy, the local fluence will become polarization dependent, which may theoretically open the possibility to image birefringence as well. However, changes in optoacoustic response due to rather slow birefringence-related fluence variations are expected to be much weaker than for dichroism.

In conclusion, we have shown that anisotropic effects can be detected optoacoustically in diffusive media and demonstrated the feasibility of PSOT. Verified in diffusive tissue-like phantoms herein, this tomographic approach has the potential to image intrinsic dichroism of materials and tissues and to investigate anisotropic characteristics associated with disease formation, such as the crystallization of molecules in tissues, and even calls for the development of new types of polarization-selective contrast agents. Polarization imaging has already developed many applications around morphological contrast mechanisms in surface or endoscopic tissue imaging, for example, skin cancer differentiation or atherosclerotic plaque characterization [13,14]. Polarization has also been associated with orientation effects in fluorescence molecules [15]. We have previously shown that multispectral optoacoustic tomography can provide in-depth high-resolution visualization of fluorescent molecules in mice [4]; therefore PSOT might be suitable for imaging polarization-dependent absorption of fluorophore probes to report on the degree of order in certain structures embedded deep in diffuse tissues. The spatial resolution in optoacoustics is not limited by the diffusion path length; therefore PSOT could propagate the *in vivo* studies of some of these phenomena deeper in tissue with superior resolution compared to the one granted by conventional polarization diffuse imaging. The method shown here was capable of accurately resolving polarized structures embedded deep in turbid medium having tissue-like optical and acoustic properties with 150 μm spatial resolution, which can also be significantly improved by using higher-bandwidth ultrasonic detectors. Finally, using reverse-contrast mechanisms, the presented method opens possibilities for light-depolarization studies in intact tissues as well as for general verification of theories of polarized light propagation in turbid media.

This study was supported in part by the National Institutes of Health (NIH) grant R01 EB00438201.

References

1. V. E. Gusev and A. A. Karabutov, *Laser Optoacoustics* (American Institute of Physics, 1993).
2. X. Wang, Y. Pang, G. Ku, G. Stoica, and L. V. Wang, Nat. Biotechnol. **21**, 803 (2003).
3. G. Ku, X. Wang, X. Xie, G. Stoica, and L. V. Wang, Appl. Opt. **44**, 770 (2005).
4. D. Razansky, C. Vinegoni, and V. Ntziachristos, Opt. Lett. **32**, 2891 (2007).
5. S. Mallidi, T. Larson, J. Aaron, K. Sokolov, and S. Emelianov, Opt. Express **15**, 6583 (2007).
6. D. Razansky and V. Ntziachristos, Med. Phys. **34**, 4293 (2007).
7. P. J. Wu and J. T. Walsh, J. Biomed. Opt. **11**, 014031 (2006).
8. J. R. Kuhn, Z. Wu, and M. Poenie, Biophys. J. **80**, 972 (2001).
9. V. Louis-Dorr, K. Naoun, P. Alle, A.-M. Benoit, and A. Raspiller, Appl. Opt. **43**, 1515 (2004).
10. L.-W. Jin, K. A. Claborn, M. Kurimoto, M. A. Geday, I. Maezawa, F. Sohraby, M. Estrada, W. Kaminsky, and B. Kahr, Proc. Natl. Acad. Sci. USA **100**, 15294 (2003).
11. M. Xu and R. R. Alfano, Phys. Rev. Lett. **95**, 213901 (2005).
12. S. G. Demos, H. Radousky, and R. Alfano, Opt. Express **7**, 23 (2000).
13. S. L. Jacques, J. R. Roman, and K. Lee, J. Biomed. Opt. **7**, 329 (2000).
14. S. K. Nadkarni, M. C. Pierce, B. H. Park, J. F. de Boer, P. Whittaker, B. E. Bouma, J. E. Bressner, E. Halpern, S. L. Houser, and G. J. Tearney, J. Am. Coll. Cardiol. **49**, 1474 (2007).
15. M. A. Rizzo and D. W. Piston, Biophys. J. **88**, L14 (2005).